

Heat conduction problems in crystal growth from the vapor

Jon Nelson

FM-15, Department of Physics, University of Washington, Seattle, Washington 98195, USA

Received 17 September 1992; manuscript received in final form 12 April 1993

When a crystal is grown or evaporated on a substrate, temperature gradients are set up in the crystal. The surface temperature of the crystal becomes non-uniform and differs from the substrate temperature. The consequences of this non-uniformity in surface temperature are analyzed for several crystal geometries. It is shown that the non-uniformity in surface temperature may drastically affect the growth rate, step spacing, and growth shape. This analysis is applied to recent experiments on ice and rare gas crystals.

1. Introduction

Crystals have been grown and evaporated on substrates to study many different surface processes. When the growth units (atoms or molecules) incorporate themselves into, or evaporate from the crystal, the latent heat flux must be conducted to, or from the underlying substrate. In this paper, we will use the term surface heating to describe this heating process for the case of growth and evaporation. Since the time scale for temperature changes in a typical laboratory crystal is much smaller than the time scale for most experiments, we will assume a steady state has been achieved. The processes that are affected by surface heating are those related to growth and evaporation rates. These include: measurements of the condensation coefficient [1–14,86], step kinetics [1,8,9,15–18], and growth shapes [19–25].

The structure of this paper is as follows: in section 2, surface heating effects on the growth/evaporation rates are calculated, in section 3, surface heating effects on the step kinetics are calculated, and in section 4 we will discuss how surface heating alters the growth shape. Throughout this paper, we will assume the growth shape is initially given.

2. Growth/evaporation rate

2.1. One-dimensional heat conduction

First consider the growth normal to the substrate of a crystal with surface temperature T_m and thickness L_m (fig. 1). The source crystal serves as a source/sink of growth units. It has a surface temperature T_s and thickness L_s . The heat flux to a crystal surface is the latent heat per molecule multiplied by the flux of vapor molecules to that surface (the heat flux into the vapor is negligible when $L_m/\lambda \ll$ chamber dimensions/ λ_{vapor} , and this condition will be assumed). The heat flux into the crystal is equal to the temperature gradient at the crystal surface multiplied by the thermal conductivity of the crystal λ :

$$\lambda \left. \frac{d}{dz} T \right|_m = HR_m/\Omega, \quad (1)$$

where R_m is the growth rate normal to the surface, H is the latent heat per molecule, and Ω is the volume occupied by one molecule in the crystal. A similar equation holds for the source crystal. For simplicity, assume that the vapor flux to the surface is determined by the Hertz-Knudsen equation. For the systems of interest for this study (ice and rare gas solids), the Hertz-Knud-

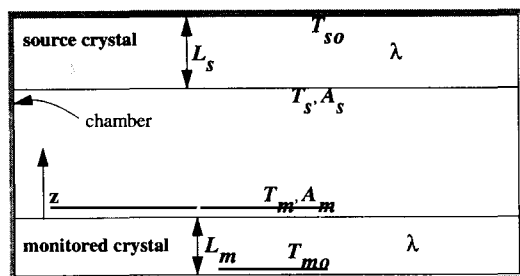


Fig. 1. Growth of a semi-infinite crystal. T and A represent temperatures and surface areas exposed to the vapor respectively.

sen equation is expected to be correct within a factor of 2 [26–32,72–76]. If surface heating/cooling effects are significant, the modifications due to this factor will be insignificant. It is convenient to define an effective temperature T_{eff} such that the chamber vapor pressure $\equiv p(T_{\text{eff}})$, p denoting the saturated vapor pressure. Since many experiments are performed at low super-/undersaturation, we will expand T_m about T_{eff} to first order:

$$R_m = \Omega \frac{B_m \lambda}{HL_m} \alpha_m^t (T_{\text{eff}} - T_m), \quad (2)$$

$$B_m \equiv \frac{L_m}{\lambda} p(T_{m0}) \frac{\bar{v}(T_{m0})}{4T_{m0}} \beta^2. \quad (3)$$

Therefore,

$$\lambda \frac{d}{dz} T \Big|_m = B_m \frac{\lambda}{L_m} \alpha_m^t (T_{\text{eff}} - T_m), \quad (4)$$

where $\bar{v}(T) = \sqrt{8kT/\pi m}$ is the vapor mean molecular speed, m is the mass of the condensing or evaporating molecule, k is Boltzmann's constant, $\beta \equiv H/kT$, and α_m^t is the probability that an incident molecule becomes incorporated into the monitored crystal lattice after striking the crystal surface (commonly called the condensation coefficient). If the heat must conduct through additional layers before reaching the thermometer, one should replace L_m/λ with $\sum L_m^n/\lambda^n$, the superscript n labeling the layer.

In the terrace–ledge–kink (TLK) model [35–39] of crystal growth, α_m^t is a product of two factors. The first factor is the sticking coefficient, which may be estimated using a trajectory model [33,34]. The second factor may be calculated using a surface diffusion model [35–39], or a Monte Carlo calculation [40,41]. If the surface is rough, the second factor equals one. The sticking coefficient should be approximately one if the surface adsorption energy is larger than the incident kinetic energy. For a vapor molecule incident on its own solid, this is usually the case. In this paper, it will be assumed to be 1. Note that the heat flux,

Table 1

Values of the parameter B_m for a few substances; data are from the following sources: metals [67,69], organic crystals [3,68], silicon [68,69], rare gas solids [57,68], ice [43,70,71]; $T_{s0} \approx T_{m0}$ has been assumed and T_L indicates the melting temperature

Substance	λ (W/m·K)	p (Pa)	\bar{v} (m/s)	β	B_m (100 μm)
Krypton	0.4 (80 K)	0.4×10^3	141.9	14.6	9.1
	0.25 ($T_L \approx 116$ K)	68.0×10^3	170.8	11.2	1199.9
Xenon	0.75 (100 K)	0.1×10^3	126.7	8.2	0.267
	0.25 ($T_L \approx 161$ K)	74.2×10^3	160.8	11.2	885.7
Naphthalene	0.71 ($T_L \approx 351$ K)	792.0	240.4	17.8	5.87
Benzene	0.85 ($T_L \approx 278$ K)	4116.1	274.0	8.1	7.35
Ice	3.3 (193 K)	0.055	476.4	31.6	1.0×10^{-3}
	2.1 ($T_L \approx 273$ K)	611.2	566.5	22.5	7.47
Silicon	22.0 (1320 K)	22.0	995.6	6.7	7.8×10^{-4}
Lead	32.0 ($T_L \approx 600$ K)	0.055	247.1	16.9	4.9×10^{-6}
Gold	250 (1300 K)	89.1	373.0	14.1	4.9×10^{-4}

and hence the vapor flux, is proportional to the temperature difference between an effective temperature (T_{eff}) and the surface of the monitored growing/evaporating crystal (T_m). However, in an experiment, the temperatures at the substrate (T_{m0} , T_{s0}), or slightly below the substrate (T_b in fig. 5), of the source crystal and the monitored crystal are measured. Therefore, the observed growth rate will be less than that given by eq. (2) with $T_{\text{eff}} = T_{s0}$, and $T_m = T_{m0}$, by a factor

$$\tilde{t} \equiv (T_{\text{eff}} - T)/(T_{s0} - T_{m0}), \quad (5)$$

with $T = T_m$. We will see in the next section that, when T varies along the surface, \tilde{t} becomes a convenient variable for describing the heat conduction process. For a semi-infinite slab (or equivalently, a finite slab with insulated sides), the temperature gradient is constant throughout the crystal, and is in the direction normal to the surface. Solving (4), and a similar equation for the source crystal, and using the definition (5),

$$\tilde{t} = \left(1 + \alpha_m^l B_m + \frac{\alpha_m^l A_m L_s B_m}{\alpha_s^l A_s L_m B_s} (1 + \alpha_s^l B_s) \right)^{-1}. \quad (6)$$

A slightly less general form of this result was previously derived by Lamb [42]. A similar result is obtained when the supersaturation is very large, and during free evaporation.

The parameters $B_{m,s}$ are proportional to both the flux of heat to the surface and the crystal thickness, but are inversely proportional to the coefficient of heat conductivity. Physically, $B_{m,s}$ represents the ratio of the latent heat flux into the crystal to the heat flux out of the crystal through conduction. Table 1 lists values of B_m for various solids, with the assumption $T_{m0} \approx T_{s0}$. The sensitivity in B_m with temperature is due to the exponential dependence of the saturated vapor pressure on temperature. The small magnitudes of B_m for silicon, lead, and gold is due to both the small magnitudes of their vapor pressures, and their relatively large thermal conductivities. In contrast, at large supersaturations ($p(T_{s0}) \gg p(T_{m0})$),

$$B_m = RL_m k \beta^2 / \Omega \lambda, \quad (7)$$

where R is the growth rate in the absence of crystal temperature gradients. Therefore, for a given R and L_m , the thermal conductivity is the controlling factor. Note the difference between (7) and (3); (3) is independent of the applied super/under saturation, while (7) is proportional to the applied super/under saturation.

It should be noted that (6) is similar to the result one obtains when an isolated sphere is growing, losing its heat to a surrounding inert gas via conduction [43–45]. We have neglected the impedance to heat flow at the crystal–substrate interface. This impedance is negligible except at very low temperatures [46]. The growth rate normal to the surface may be written;

$$R_m = \alpha R_m^{hk}, \quad (8)$$

$$\alpha \equiv \left[\frac{1}{\alpha_m^l} + B_m + \frac{A_m}{A_s} \left(\frac{1}{\alpha_s^l} + B_s \right) \right]^{-1}, \quad (9)$$

where Ω is the volume per molecule in the crystal, α is the growth rate divided by the Hertz–Knudsen growth rate,

$$R_m^{hk} = \Omega p(T_{s0}) \bar{v}(T_{s0}) \sigma / 4kT_{s0}$$

without surface heating, and

$$\sigma = \beta(T_{s0} - T_{m0}) / T_{s0}$$

is the applied supersaturation. The growth rate has been factorized in this manner because many authors equate α with α_m^l [1–9,11]. Examination of (9) and table 1 shows that α_m^l values derived in this manner will be too small in many cases. In section 2.3, we will discuss this in more detail.

2.2. Three-dimensional effects

The circular disk shape (fig. 2) will be treated first. This shape is an approximation to a hexagonal plate. Consider the case of a crystal with all exposed vicinal faces above the roughening temperature. For such a crystal, there is no energy barrier for ledge formation. Therefore, the local growth rate is determined only by the local surface temperature. We may solve for the reduced temperature using the method of separation of variables with eq. (4) as the top and side surface

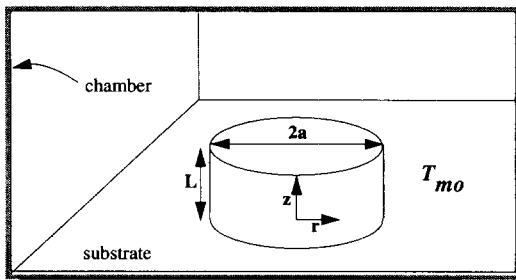


Fig. 2. Geometry of a growing disc.

boundary condition and $T = T_{m0}$ on the bottom surface. The results from such a calculation will depend on the parameter B_m and the aspect ratio L/a . The special case of $B_m = 2$ and $L = a$ is plotted in figs. 3a and 3b. The surface temperature is highest at the top edge (during growth) and lowest at the base. The resulting non-uniformity of surface temperature translates into a

non-uniformity in surface supersaturation through the relation

$$\sigma_s = \beta(T_{\text{eff}} - T) / T_{\text{eff}}$$

The crystal grows fastest where it meets the substrate and slowest at the top edge. Therefore, a crystal prepared with an initial disc shape will grow into a flatter, rounder shape.

Now consider the case when the substrate temperature is below the roughening temperature of all exposed vicinal faces. Crystals grown in such an environment have been observed to retain the same exposed vicinal faces [1,8–10]. Therefore, surface processes must compensate for the non-uniformity in surface supersaturation to produce a uniform growth rate over the vicinal faces. This can be accomplished in one of two ways; non-uniformity in the distribution of growth sites, or a net migration of the mobile surface molecule from the colder to the warmer parts of the crystal surface. This latter mechanism appears unlikely, given the absence of a physical mechanism. Therefore, in the rest of this paper, only variations in the distribution of growth sites will be considered. Since the growth process proceeds by the formation and motion of kinks along a step, and the motion of the steps across the vicinal face, a non-uniformity in the distribution of growth sites can occur by a non-uniformity in the kink density, the ledge density, or both.

The simplest mechanism for ensuring a constant normal growth rate along a vicinal face is to assume that the region of lowest surface supersaturation contains the source of the steps. This source of steps is unlikely to be due to nucleation, since nucleation is expected to occur first at the regions of highest surface supersaturation (although there is some experimental evidence to the contrary [82]). Therefore, a self-perpetuating step source is needed, such as a spiral step, or a stacking fault [83]. At higher applied supersaturations, nucleation of ledges in the higher surface supersaturation regions may begin to compete with the self-perpetuating step sources, and eventually, at high enough applied supersaturations, may dominate the growth process. Note that the normal growth rate along a vicinal face may be

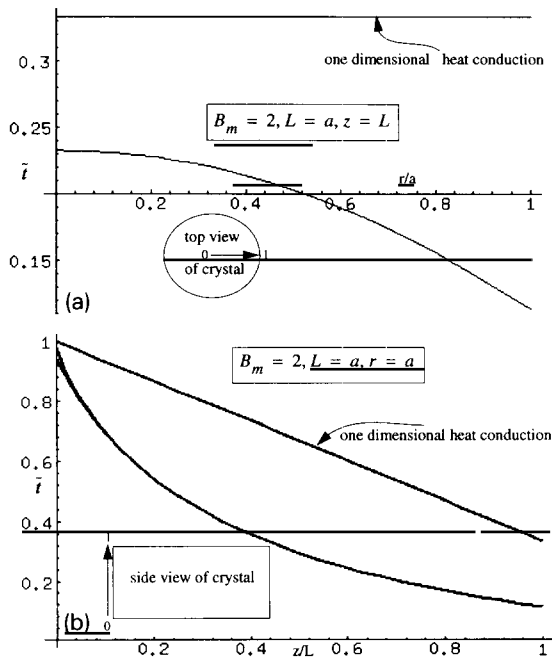


Fig. 3. Surface temperatures along the top and side of a growing disc when the crystal is not constrained to retain its shape. $\alpha'_m = 1$ has been assumed. The one-dimensional approximation is the result from eq. (6) with $A_m/A_s = 0$.

Table 2
 The shape parameters for estimating the growth rates of a finite crystal; L_x and L_y are the dimensions of the rectangle, γ_c is Catalan's constant with a numerical value of ≈ 0.915966 , $s = L_b/a$, and $s_{x,y} = L_b/L_{x,y}$; approximate forms for f_F are $e^{-s/2}$ and $e^{-(s_x+s_y)/2}$ for crystals with a circular base and a rectangular base, respectively

Shape	f_c	f_c approximation	f_c^1	f_F
Cylinder	$1 + \frac{2}{\pi^2} \sum_{n=0}^{\infty} \frac{-1^n I_0(\alpha_n a)}{(n + \frac{1}{2})^2} I_1(\alpha_n a)$	$1 + \frac{L/a}{\tanh[(L/a)/(8\gamma_c/\pi^2)]}$	$1 + 2L/a$	$\frac{2}{s} \int_0^{\infty} dx \frac{J_1^2(x)}{x^2} \tanh(sx)$
Rectangle	$1 + \frac{2}{\pi^2} \sum_{n=0}^{\infty} \frac{-1^n}{(n + \frac{1}{2})^2} \times \coth\left(\frac{\alpha_n L_x}{2}\right) + \coth\left(\frac{\alpha_n L_y}{2}\right)$	$1 + \frac{L/2L_x}{\tanh[(L/2L_x)/(8\gamma_c/\pi^2)]} + \frac{L/2L_y}{\tanh[(L/2L_y)/(8\gamma_c/\pi^2)]}$	$1 + 2L/L_x + 2L/L_y$	$\frac{16}{\pi^2} \int_0^{\infty} dx \int_0^{\infty} dy \sin^2\left(\frac{x}{2}\right) \sin^2\left(\frac{y}{2}\right) \times \frac{\tanh\left\{\left[(s_x x)^2 + (s_y y)^2\right]^{1/2}\right\}}{x^2 y^2 \left[(s_x x)^2 + (s_y y)^2\right]^{1/2}}$
Sphere	1.29559	1.29559	1.997	$\frac{2}{s} \int_0^{\infty} dx \frac{J_1^2(x)}{x^2} \tanh(sx)$

constant even if the step source is in a region of higher surface supersaturation. This has been discussed previously [53,84].

Now introducing the reduced coordinates $\tilde{r} \equiv r/a$ and $\tilde{z} \equiv z/L$, and combining eq. (4) with definitions (3) and (5),

$$\frac{d}{dx} \tilde{i}(\tilde{r}, \tilde{z}) \Big|_m = - \frac{B_m}{L} \alpha_m^t(\tilde{r}, \tilde{z}) \tilde{i}(\tilde{r}, \tilde{z}) \Big|_m, \quad (10)$$

where $x = r$ or z depending on the surface where this boundary condition is being evaluated. Except when stated otherwise, in the rest of this paper we will assume $T_{\text{eff}} = T_s = T_{s0}$, $A_m/A_s = 0$, and an isotropic thermal conductivity. Since the right-hand side of (10) is proportional to the growth rate normal to the surface, which is assumed to be constant along the surface, it must be independent of surface position. Therefore, we will assume it is equal to its value evaluated at the step source. We will assume that the step source is at the top edge for both the top and the side face. Therefore,

$$\frac{d}{dx} \tilde{i}(\tilde{r}, \tilde{z}) \Big|_m = - \frac{B_m}{L} \alpha_m^t(1, 1) \tilde{i}(1, 1), \quad (11)$$

$$\tilde{i}(\tilde{r}, 0) = 1. \quad (12)$$

Eqs. (11) and (12) become the new boundary conditions for the heat conduction problem. Eq. (11) contains an unknown constant $\tilde{i}(1, 1)$. This will be solved for by insisting on self-consistency. The calculation is in appendix A. The result is

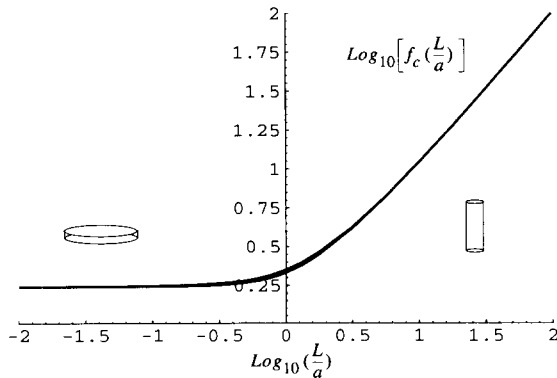


Fig. 4. The shape factor for a cylindrical disc. The lower curve is the approximation given in table 2.

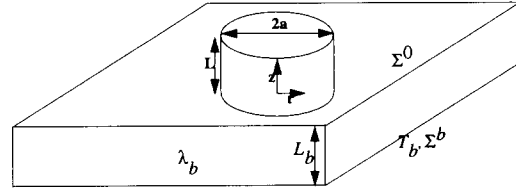


Fig. 5. Geometry of a growing disc on a semi-infinite slab.

identical to eq. (6), with the substitution; $B_m \rightarrow B_m f_c(L/a)$. The shape parameter f_c is plotted in fig. 4. Note that it does not approach 1 as L/a approaches 0. Instead it has a limiting value of 1.74 because there is always surface heating along the sides of the crystal. The resulting α is

$$\alpha = \left(\frac{1}{\alpha_m^t(1, 1)} + B_m f_c(L/a) \right)^{-1}. \quad (13)$$

In most experiments the heat must also be conducted through a thin substrate layer before reaching the thermometer. The heat conduction problem for conduction through the crystal and a finite substrate (fig. 5) may be approximated if we replace the heat flux through the base of the crystal with its average value, and assume the crystal base has a uniform temperature (fig. 6);

$$\alpha = \left(\frac{1}{\alpha_m^t(1, 1)} + B_m f_c(L/a) + B^1 f_c^1(L/a) f_F(L_b/a) \right)^{-1}, \quad (14)$$

where B^1 is identical to B_m , except $L/\lambda \rightarrow L_b/\lambda_b$, L_b and λ_b being the thickness and thermal conductivity of the base, and $f_c^1(x) = 1 + 2x$. The function f_F is given in table 2.

We have performed similar calculations for a growing rectangular slab and a hemisphere. A compilation of the results, along with some useful

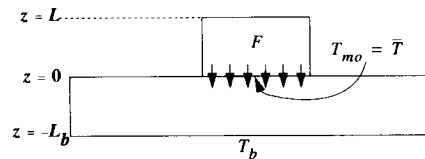


Fig. 6. Cross section of a growing disc on a semi-infinite slab.

approximations, are listed in table 2. The surface heating for a given crystal thickness becomes larger when the width decreases. This is because the heat must be conducted through a narrower region. The shape factor f_c equals 2.24 for the cylinder when the crystal radius is equal to its thickness and equals 2.70 for a cube of equal volume and thickness. As expected, the shape with the sharpest corners will grow/evaporate the most slowly (if the step source is at the outermost corner).

The calculations presented above have only considered the heat conduction through the monitored crystal. In general the heat conduction through the source crystal must also be taken into account. We expect that surface heating/cooling of the source crystal will bring new terms to the denominators of eqs. (13) and (14) which are identical to the existing terms, but with the substitution $m \rightarrow s$, and a prefactor A_m/A_s (as in the third term in the denominator of eq. (9)). This is because the derivation above also applies to surface cooling during evaporation. When one of the crystals is growing, the other is evaporating, but each must conduct heat between its surface and its substrate. Note that the combined effects of heat conduction in the source and monitored crystal change the magnitude, not the sign, of the surface supersaturation. A previous experiment [85] had measured sublimation when growth was expected. This behavior cannot be due to heat conduction. Note that radiative heating/cooling may shift the equilibrium temperature to a lower/higher temperature, but the magnitude of the shift is independent of supersaturation.

2.3. Comparison with experiment

The results above may be used to reanalyze recent experiments on the growth rate of ice from the vapor [1–10,86]. A compilation of the results is plotted in fig. 7, along with curves plotted using eq. (13). The measured reduction in growth rate may be approximately fit assuming values of the crystal thickness between 50 and 200 μm . The exact crystal sizes present during measurement were generally not reported by the authors. However, the experiments at temperatures greater

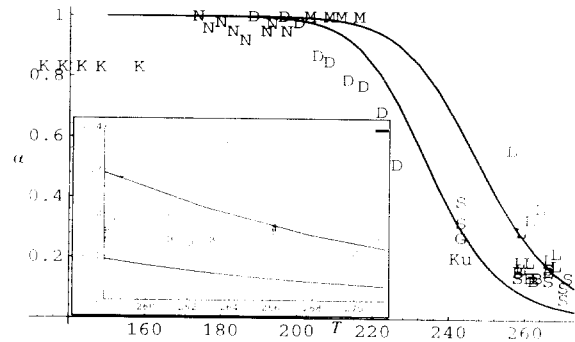


Fig. 7. Compilation of growth rate experiments on ice crystals. The letters indicate the researchers: S = Sei and Gonda [8], B = Beckmann and Lacmann [1], L = Lamb [10] (calculated by Beckmann and Lacmann [1]), Ku = Kuroda and Gonda [2], G = Gonda and Koike [86], D = Davy and Somorjai [5], M = Kramers and Stemerding [4] (corrected for molecular flow impedance by Cammenga et al. [12]), N = Nitsch and Viardot [3], K = Koros et al. [6]. Also shown is the estimate from eq. (13) with $L = a = 50$ and $100 \mu\text{m}$. Inset shows the region near 273 K.

than 230 K were on crystals with thicknesses probably near these two values.

This analysis may also be compared with a recent experiment on the growth rate of xenon and krypton [11]. The crystals were approximately 20 μm thick and more than three times as wide. Since these crystals were observed to be rounded, the crystal shape probably flattened as it grew, and hence, the analysis presented above does not strictly apply. This will be considered in more detail in section 4. Nevertheless, it seems quite reasonable that the growth rate should be given by eq. (13) with the function f lying between 1 and its value for a sphere. Assuming $f = 1$, the calculated value of α for xenon at 161 K is 0.0054, and for krypton at 115 K, $\alpha = 0.0040$. These are fairly close to the measured values of 0.00835 and 0.00619. Note that the ratio of the two values are 1.35 ± 0.2 (measured), and 1.36 ± 0.3 (calculated), which is approximately independent of crystal thickness. The uncertainty in the calculated value is due to the uncertainty in the heat conductivity [57]. These two observations together suggest that the measured reduction in growth rate was due to surface heating.

In both of these cases, the authors neglected the contributions from the second and third terms

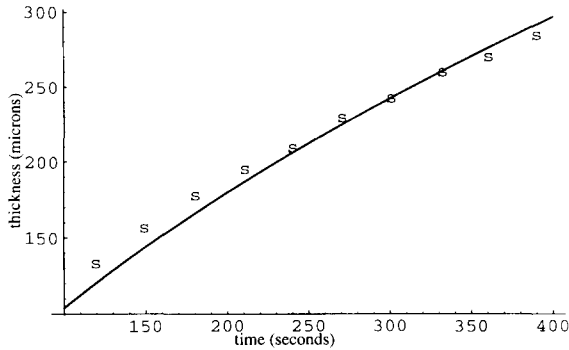


Fig. 8. Size of an ice crystal growing at -30°C , 2.7% supersaturation. Also shown are the data of Sei and Gonda [8].

in the denominator of (14), and concluded that the measured decrease in growth rates (α) were due to the condensation coefficient (α_m^t). The results of this section suggest that the measured growth rates may be due to surface heating instead, and thus the condensation coefficient may be equal to one, as is theoretically expected [12]. The analysis given above does not rule out the possibility that α_m^t may be less than one (in the linear growth regime). Instead it must be closer to one than the measurements had suggested.

The thickness of the crystal as a function of time is easily calculated. It is given by:

$$L(t) = \left(C^2 + 2CL(0) + L^2(0) + 2\frac{R_m^{hk}}{C_2}t - C \right)^{1/2}, \quad (15)$$

where $C_2 \equiv B_m f_c / L_m$ and $C \equiv (1/\alpha_m^t + B^1 f_c^1) / C_2$. The special case $\alpha_m^t = 1$, $f_c = 1$, $B^1 = 0$, $L(0) = 0$, and $\sigma = 0.027$, $T_s = -30^{\circ}\text{C}$ is shown in fig. 8. It can be seen that, at least over small size ranges, the curvature is very small. Note that if (1) α_m^t is the same on all faces and (2) the amount of surface migration of mobile surface molecules from one face to another is small [15], then the crystal width should grow at the same rate as the thickness. In fact, this was assumed in the derivation of (15). Slight curvatures, which can be fit to (15), have appeared in the data on ice [2,8] and krypton [51]. Note also that as B^1 increases, the curvature will decrease even further. It had been

argued that a linear relationship between crystal size and time indicates that surface-heating is insignificant [2,8]. Since the actual curvature can be very small, this is not the case.

3. Step kinetics

3.1. Step spacing at constant supersaturation

It was argued in section 2 above that the ledge kinetics must compensate for the surface heating. During growth, this requires that the step spacing increase in the colder regions of the crystal. The dependence of α_m^t on the step spacing (in the absence of vapor diffusion, and assuming a high density of kinks) is given by [38,39]

$$\alpha_s = (2/\hat{y}) \tanh(\hat{y}/2), \quad (16)$$

where \hat{y} = ledge spacing divided by $\sqrt{D_s \tau_s}$, D_s is the surface diffusion constant and τ_s is the mean surface residence time. For simplicity, the step

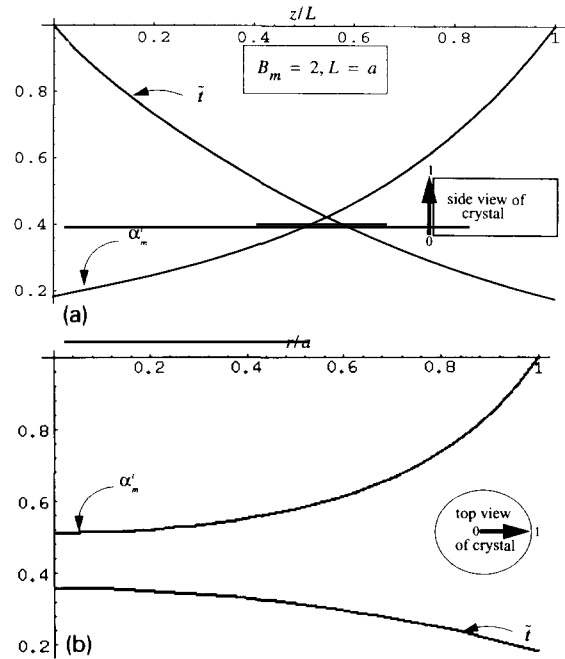


Fig. 9. Surface heating and surface diffusion contributions to the reduction in growth rate along the top (b) and side (a) of a cylindrical disc.

capture coefficients from the top and bottom terrace have been assumed to be large. Figs. 9a and 9b show a plot of $\tilde{l}(\tilde{r}, \tilde{z})$, and the required value of α_m^l ;

$$\alpha_m^l(\tilde{r}, \tilde{z}) = \alpha_m^l(1, 1) \tilde{l}(1, 1) / \tilde{l}(\tilde{r}, \tilde{z}), \quad (17)$$

for the case when $\alpha_m^l(1, 1) = 1$. This expression may then be used, along with (16), to solve for \hat{y} along the top, and sides of a disc shaped crystal. The special case $B_m = 2$, $L = a$ is plotted in fig. 10. The step spacing equals 0 at the corners because $\alpha_m^l(1, 1) = 1$ has been assumed. The predicted decrease in step spacing at the corners furthest from the substrate has been observed [42,49,50]. During growth, α_m^l depends on the surface supersaturation σ_s , which differs from the applied supersaturation $\sigma = \beta(T_{s0} - T_{m0})/T_{s0}$. Hereafter, when σ_s , or α_m^l are used, it is assumed that they are evaluated at the step source.

3.2. Extracting surface parameters from growth rate data

Eq. (16), combined with the BCF relation $2/\hat{y} = \sigma_s/\sigma_1$ [39], gives the frequently used expression relating α_m^l and σ_s for a spiral step source:

$$\alpha_m^l = (\sigma_s/\sigma_1) \tanh(\sigma_1/\sigma_s). \quad (18)$$

This expression allows one to extract the parameter σ_1 from the growth rate curve, provided one knows the surface supersaturation. In appendix B, a method is introduced which allows

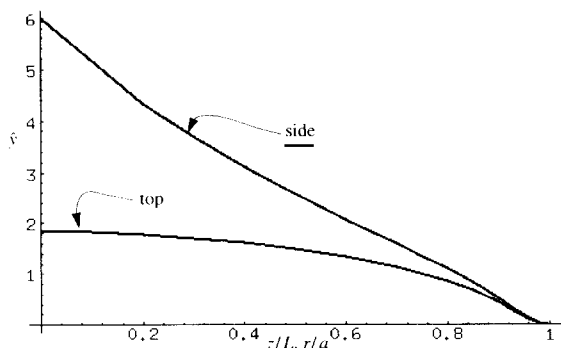


Fig. 10. Normalized ledge spacings along the top and side of a growing cylinder. The condensation coefficient at the top edge is assumed equal to 1.

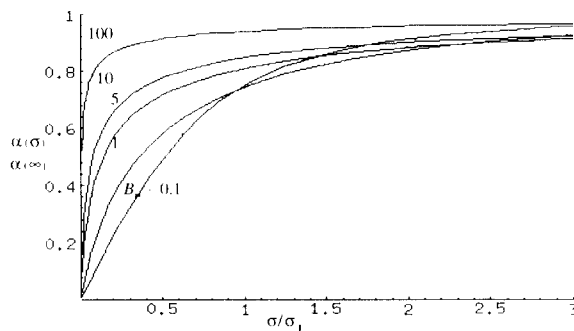


Fig. 11. Normalized growth rate at small supersaturations for a cylindrical disc.

one to calculate the surface supersaturation $\sigma_s = \sigma\alpha/\alpha_m^l$. Using this method, α_m^l versus σ has been plotted in fig. 11 for several values of B_m . When B_m is large, the surface heating drastically changes the growth curve. The change in the growth curve is due to an exchange in importance of the two terms in the denominator of (13). As the supersaturation is lowered, the surface kinetics (18) becomes more important. As the surface kinetics reduce the growth rate, the surface heating effect is reduced. This trade-off, or exchange, between surface kinetics and surface heating prevents the growth rate from decreasing rapidly until the surface heating effect becomes negligible. When this happens, the growth rate decreases with σ much more quickly. Therefore, as B_m increases, the applied supersaturation at which the growth rate becomes linear in σ decreases. Equivalently, the limiting slope of $\alpha(\sigma)/\alpha(\infty)$ as $\sigma \rightarrow 0$ increases with B_m . Using (13), (18) and (27), the limiting slope is given by

$$\frac{1 + B_m f_c(L/a) + B^1 f_c^1(L/a)}{\sigma_1}. \quad (19)$$

However, if surface heating had been neglected, the second and third terms in the numerator would not appear. Therefore, if one had extracted σ_1 from the data in this manner, the actual value would differ from the measured value in the following way:

$$\sigma_1^{\text{actual}} = \sigma_1^{\text{measured}} / \alpha = \text{constant}. \quad (20)$$

Eq. (20) is general, and applies to all α which are influenced by surface heating, vapor diffusion, vapor flow impedance [47], or any combination of these. Evidence for this relationship can be found in recent experiments on ice growth [9]. The growth rate of single ice crystals at -15°C was measured for ice crystals with dimensions of approximately 200 and 400 μm . When the larger ice crystal was measured, $\sigma_1^{\text{measured}} = 1.06$ and $1/\alpha = 11.23$, while the smaller crystal gave the values 1.8 and 6.67. The product of each set of numbers is the actual value of σ_1 and gives 11.9 for the larger crystal, while the smaller crystal has the value 12.0. Note that neither σ_1 nor α_m^t should depend on crystal size. Therefore, the analysis presented in this section may be used to correct experimentally derived values of σ_1 . For the case of ice, the original and corrected values for various temperatures are given in table 2.

4. Growth shape

4.1. The rounding transition

Surface processes can only keep the crystal face vicinal between two points on the face when the surface supersaturation difference between these two points is not too large. Above a critical surface supersaturation difference, the shape of the crystal will change. For instance, ice crystals grown on a substrate in a single component vapor have been observed to become flatter and rounder when the applied supersaturation becomes greater than a certain value [1,42], while dendritic growth is observed at large applied supersaturations when the growth units must diffuse through an inert foreign gas [15,53]. These two transitions can be related in the following way. Consider the case of dendritic ice crystals grown in an inert foreign gas. These form only at certain temperatures, and at external supersaturations above approximately 15% [15,53]. At lower supersaturations hexagonal plates are formed (see fig. 12). One can easily estimate the surface supersaturation difference $\Delta\sigma_s$ between a corner and the center of an edge face by assuming a spherically symmetric diffusion field centered on the crystal.

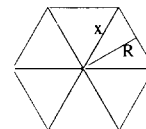


Fig. 12. Estimation of the supersaturation between the corner, and the center of an edge of a hexagonal plate crystal growing in 1 atm of air.

This predicts $\Delta\sigma_s \leq 2\%$. Beckmann and Lacmann [1], growing ice on a substrate in a pure vapor environment, observed the crystal edges becoming rounder when the applied supersaturation was greater than approximately 1.3%. The largest difference in surface supersaturation for a circular disc (approximately a hexagonal plate) occurs between the substrate and the top edge. At the base of the crystal, the surface supersaturation equals the applied supersaturation ($T = T_{m0}$), while at the top corner of the crystal, the surface supersaturation is given by $\sigma_s = \sigma\alpha/\alpha_m^t$. Assuming $\alpha_m^t = 1$ and $B^t = 0$, the difference in surface supersaturation is $\approx 1.1\%$, which agrees fairly well with the dendritic transition estimate given above.

In the above example, it was argued that the transition to rounded growth on a substrate depends on the magnitude of B_m . A larger value of B_m causes a transition at a lower value of applied supersaturation. Experiments on rare gas crystals at low temperature (smaller values of B_m) found growth shapes with exposed vicinal faces [25], while similar experiments at higher temperatures (very large values of B_m) found only rounded growth shapes [11]. It was argued that this was due to the roughening transition on the exposed faces. Since the magnitudes of B_m are so large for this system, the transition may be strongly influenced by surface heating.

4.2. Growth of a rounded crystal

When the surface supersaturation difference between two points on a vicinal face becomes larger than a critical value, the boundary of this face will begin to grow at a slower rate. For instance, consider the disc-shaped crystal. When the top edge becomes rounded, the top face, and

Table 3

The measured [8] and corrected values of the limiting slope parameter (σ_l) for ice crystal growth ($\alpha_m^1 \rightarrow \sigma_c/\sigma_l$ as $\sigma_c \rightarrow 0$) the first column. $1 + fB$ was derived from the measured reduction in growth rate: when the prism and basal facets had different values, the average value was used

Temperature (°C)	$1 + fB$	$\sigma_l(\text{meas}) \{0001\} (\%)$	$\sigma_l(\text{corr}) \{0001\} (\%)$	$\sigma_l(\text{meas}) \{10\bar{1}0\} (\%)$	$\sigma_l(\text{corr}) \{10\bar{1}0\} (\%)$
-1.9	7.14	0.56 ± 0.1	4.0	0.5	3.57
-3.1	11.11	0.35	3.89	0.38	4.22
-7	6.67	2.5	16.67	2.2	14.67
-15	6.67	0.5	3.33	1.8	12.0
-30	2.82	1.7	4.79	2.7	7.61

the side face can no longer grow at the same rate. If the radius of curvature of the edge is much smaller than the radius of the crystal, the growth rates of both faces may be calculated. Since the magnitude of \tilde{r} is generally larger along the side of the crystal than along the top of the crystal (figs. 9a and 9b), the top face will likely grow slower than the bottom face. Therefore, after this critical size/applied supersaturation is reached, the rounded crystal will begin to spread out and become flatter in appearance [42].

5. Conclusions

Several effects of surface heating on crystal growth have been presented. Some of them, such as a reduction in growth rate, and a reduction in the transition supersaturation for linear growth have been shown to quantitatively agree with experiment. Other effects, such as the variation in ledge spacing across a face, and the transition supersaturation for edge rounding, have been shown to agree qualitatively with experiment. It is argued that the measured reduction in growth rates (α) of ice, xenon, and krypton in a pure vapor environment are due to surface heating instead of the condensation coefficient (α_m^1). Therefore, the experimental results are consistent with a condensation coefficient of unity. One may turn the argument around, and measure growth rates to infer thermal conductivities. Such a measurement will rest on the assumption that $\alpha_m^1 = 1$. The Langmuir method for measuring vapor pressures depends on this same assumption. For instance, if this assumption is applied to the growth of adamantane [78], a thermal conductivity of

0.16 W/m · K is deduced. This is a reasonable value for a plastic crystal.

The role of heat conduction during crystal growth has become known as a secondary effect [12,54]. We have discussed one other secondary effect: vapor flow impedance. Another common secondary effect is impurity adsorption [55,56]. A common feature of secondary effects is alteration of growth and evaporation rates. In this regard, our understanding of condensation effects on solids may be following the long history of condensation coefficient measurements of liquids. Early measurements found small condensation coefficients. Later experimenters were more careful about avoiding secondary effects, and instead measured coefficients near unity [54]. This same trend is occurring in the measurements of condensation coefficients of solids [13]. The only known exceptions to this trend are measurements on materials which must undergo a chemical change upon condensation or evaporation such as arsenic [14]. Some authors [79,80] have reported larger values of the evaporation coefficient at temperatures just above the melting temperature compared with the values just below the melting temperature. This is possibly due to convective heat transport in the liquid, which will drastically reduce the surface heating if the crystal/liquid thickness is larger than a convective cell dimension [54,81].

Acknowledgments

This research was supported by NASA global change fellowship #NGT30004. The author thanks M. Baker and J.R. Ferron for valuable suggestions.

Appendix A

Let $\Theta \equiv \tilde{t} - 1$. This gives the bottom surface a homogeneous boundary condition. By splitting Θ into 2 parts, where each part has only 1 non-homogeneous boundary condition, the technique of separation of variables may be used. The result is

$$\Theta = -B\alpha_m^t \tilde{t}(1, 1) \left[\frac{z}{L} + \frac{2}{\pi^2} \sum_{n=0}^{\infty} \frac{1}{(n + 1/2)^2} \times \frac{I_0\left(x_n \frac{r}{L}\right)}{I_1\left(x_n \frac{a}{L}\right)} \sin\left(x_n \frac{z}{L}\right) \right], \quad (21)$$

where $x_n \equiv (n + 1/2)\pi$, and $I_{0,1}$ are the modified Bessel functions [77]. If this expression is evaluated at the top corner, $\tilde{t}(1, 1)$ may be extracted:

$$\tilde{t}(1, 1) = \frac{1}{1 + \alpha_m^t Bf(L/a)}, \quad (22)$$

$$f_c(L/a) \equiv 1 + \frac{2}{\pi^2} \sum_{n=0}^{\infty} \frac{-1^n}{(n + 1/2)^2} \frac{I_0(x_n a/L)}{I_1(x_n a/L)}. \quad (23)$$

Appendix B

Eqs. (13) and (14) can be put in the form:

$$R_m = \frac{\sigma \hat{R}}{1/\alpha_m^t(\sigma_s) + 1/2Z}, \quad \hat{R} \equiv \frac{R_m^{hk}(\sigma)}{\sigma}, \quad (24)$$

where all terms in the denominator except $1/\alpha_m^t$ have been lumped into $1/2Z$. Since the definition of σ_s requires that $R = \sigma_s \hat{R} \alpha_m^t$, it follows that

$$\sigma_s = \frac{\sigma}{1 + \alpha_m^t(\sigma_s)/2Z}. \quad (25)$$

Using (18), this can be “solved” for α_m^t to obtain

$$\alpha_m^t(\sigma_s) = \left[Z^2 + 2Z \frac{\sigma}{\sigma_1} \tanh\left(\frac{1 + \alpha_m^t(\sigma_s)/2Z}{\sigma/\sigma_1}\right) \right]^{1/2} - Z, \quad (26)$$

which can be iterated to find α_m^t . Consider the following limiting cases:

Case (1), $\sigma/\sigma_1 \ll 1$, $\tanh \rightarrow 1$. Therefore:

$$\alpha_m^t(\sigma_s) = \sqrt{Z^2 + 2Z \frac{\sigma}{\sigma_1}} - Z. \quad (27)$$

Case (2), $\sigma/\sigma_1 \gg 1 - 1/2Z$:

$$\alpha_m^t = 1. \quad (28)$$

Cases (1) and (2) are both realized by starting with $\alpha_m^t = 1$ in the right-hand side of (26). It has been found that after 3 or less iterations, the result converges to 3 digit accuracy when this starting point is used.

References

- [1] W. Beckmann and R. Lacmann, J. Crystal Growth 58 (1982) 433.
- [2] T. Kuroda and T. Gonda, J. Meteor. Soc. Japan 62 (1984) 563.
- [3] W. Nitsch and K. Viardot, Chemie-Ing.-Tech. 40 (1968) 1159.
- [4] H. Kramers and S. Stemerding, Appl. Sci. Res. A 3 (1953) 73.
- [5] J.G. Davy and G.A. Somorjai, J. Chem. Phys. 55 (1971) 3624.
- [6] R.M. Koros, J.M. Deckers, R.P. Andres and M. Boudart, Chem. Eng. Sci. 21 (1966) 941.
- [7] A. Davis and R.F. Strickland-Constable, in: Proc. Intern. Symp. on Condensation and Evaporation of Solids, Dayton, OH, 1962, p. 665.
- [8] T. Sei and T. Gonda, J. Crystal Growth 94 (1989) 697.
- [9] T. Gonda, Y. Matsura and T. Sei, in: Proc. 3rd Topical Meeting on Crystal Growth Mechanism, Tokyo, 1990, p. 21.
- [10] D. Lamb and P.V. Hobbs, J. Atmos. Sci. 28 (1971) 1506.
- [11] M. Maruyama, J. Crystal Growth 94 (1989) 757.
- [12] H.K. Cammenga, H.-J. Petrick and F.W. Schulze, J. Crystal Growth 55 (1981) 351.

- [13] J.C.A. Offringa, C.G. de Kruif, P.J. van Ekeren and M.H.G. Jacobs, *J. Chem. Thermodyn.* 15 (1983) 681.
- [14] G.M. Rosenblatt, *Acc. Chem. Res.* 9 (1976) 169.
- [15] B.J. Mason, G.W. Bryant and A.P. Van den Heuvel, *Phil. Mag.* 8 (1963) 505.
- [16] J. Hallett, *Phil. Mag.* 6 (1961) 1073.
- [17] T. Kobayashi, in: *Proc. Conf. on Physics of Snow and Ice*, Hokkaido Univ., Sapporo, 1967, p. 95.
- [18] Y. Furukawa, M. Yamamoto and T. Kuroda, *J. Crystal Growth* 82 (1987) 665.
- [19] U. Nakaya, *Snow Crystals* (Harvard Univ. Press, Cambridge, MA, 1954).
- [20] M. Elbaum, *Phys. Rev. Letters* 67 (1991) 2982.
- [21] T. Gonda and T. Koike, *J. Crystal Growth* 56 (1982) 259.
- [22] P. van der Sluis and J. Kroon, *J. Crystal Growth* 104 (1990) 310.
- [23] E. van der Voort, *J. Crystal Growth* 100 (1990) 539.
- [24] M. Isshiki, M. Piechotka and E. Kaldis, *J. Crystal Growth* 102 (1990) 344.
- [25] M. Maruyama, *J. Crystal Growth* 89 (1988) 415.
- [26] T. Ytrehus, *Phys. Fluids* 26 (1983) 939.
- [27] R.E. Sampson and G.S. Springer, *J. Fluid Mech.* 36 (1969) 577.
- [28] R.W. Schrage, *A Theoretical Study of Interphase Mass Transfer* (Columbia Univ. Press, New York, 1953).
- [29] Y. Sone and Y. Onishi, *J. Phys. Soc. Japan* 44 (1978) 1981.
- [30] Y. Onishi, *J. Fluid Mech.* 163 (1986) 171.
- [31] M. Bhandarkar and J.R. Ferron, *Ind. Eng. Chem. Res.* 30 (1991) 998.
- [32] J.R. Ferron, *Ind. Eng. Chem. Res.* 25 (1986) 594.
- [33] E.W. Kuipers, M.G. Tenner, M.E.M. Spruit and A.W. Kleyn, *Surface Sci.* 205 (1988) 241.
- [34] R.B. Gerber, *Chem. Rev.* 87 (1987) 29.
- [35] R. Ghez and S.S. Iyer, *IBM J. Res. Develop.* 32 (1988) 804.
- [36] A.K. Myers-Beaghton and D.D. Vvedensky, *Phys. Rev. A* 44 (1991) 2457.
- [37] V.N. Men'shov and E.T. Klimenko, *Soviet Phys.-Cryst.* 27 (1982) 462.
- [38] R. Ghez and G.H. Gilmer, *J. Crystal Growth* 21 (1974) 93.
- [39] W.K. Burton, N. Cabrera and F.C. Frank, *Phil. Trans. Roy. Soc. London A* 243 (1951) 299.
- [40] J.D. Weeks and G.H. Gilmer, *Advan. Chem. Phys.* 40 (1978) 157.
- [41] R.F. Xiao, J. Iwan, D. Alexander and F. Rosenberger, *J. Crystal Growth* 109 (1991) 43.
- [42] D. Lamb, PhD Thesis, University of Washington, Seattle, WA (1970) p. 154.
- [43] H.R. Pruppacher and J.D. Klett, *Microphysics of Clouds and Precipitation* (Reidel, Dordrecht, 1978) p. 448.
- [44] N. Fukuta and L.A. Walter, *J. Atmos. Sci.* 27 (1970) 1160.
- [45] T. Kuroda, *J. Meteor. Soc. Japan* 62 (1984) 552.
- [46] W.A. Little, *Can. J. Phys.* 37 (1959) 334.
- [47] J. Nelson, to be published.
- [48] A. Seeger, *Phil. Mag.* 44 (1953) 1.
- [49] K. Onuma, personal communication.
- [50] T. Sei, personal communication.
- [51] M. Maruyama, personal communication.
- [52] R. Gomer, *Rept. Progr. Phys.* 53 (1990) 917.
- [53] F.C. Frank, *Contemp. Phys.* 23 (1982) 3.
- [54] H.K. Cammenga, in: *Current Topics in Materials Science*, Vol. 5, Ed. E. Kaldis (North-Holland, Amsterdam, 1980) p. 335.
- [55] A.A. Chernov, *Soviet Phys.-Usp.* 4 (1961) 116.
- [56] M. Kasuga, in: *Proc. 2nd Topical Meeting on Crystal Growth Mechanism*, Tokyo, 1989, p. 91.
- [57] M.L. Klein and J.A. Venables, *Rare Gas Solids 2* (Academic Press, London, 1977).
- [58] H.-W. Fink and G. Ehrlich, *Surface Sci.* 143 (1984) 125.
- [59] H.-W. Fink and G. Ehrlich, *Surface Sci.* 173 (1986) 128.
- [60] J. Hallett, *Phil. Mag.* 6 (1961) 1073.
- [61] S.H. Algie, *J. Chem. Phys.* 69 (1978) 538.
- [62] G.M. Rosenblatt, *J. Phys. Chem.* 71 (1967) 1327.
- [63] G. Burrows, *Vacuum* 15 (1965) 389.
- [64] P. Clausing, *Ann. Physik* 12 (1932) 961.
- [65] A.S. Berman, *J. Appl. Phys.* 36 (1965) 3356.
- [66] D.H. Davis, *J. Appl. Phys.* 30 (1960) 1169.
- [67] C.B. Alcock, V.P. Itkin and M.K. Horrigan, *Can. Met. Quart.* 23 (1984) 309.
- [68] *CRC Handbook of Chemistry and Physics*, 73rd ed. (CRC Press, Boca Raton, FL, 1993).
- [69] C.Y. Ho, R.W. Powell and P.E. Liley, *Physical and Chemical Reference Data* 3, Suppl. 1 (1974).
- [70] P.V. Hobbs, *Ice Physics* (Clarendon, Oxford, 1974).
- [71] A.L. Buck, *J. Appl. Meteor.* 20 (1981) 1527.
- [72] A.G. Gnedovets and A.A. Uglov, *Teplotiz. Vysok. Temp.* 26 (1988) 778.
- [73] A.J. Sartor, R.E. Balzhiser and R.E. Barry, *Chem. Eng. Progr. Symp. Ser.* 102 (1970) 26.
- [74] J.R. Ma, *Ind. Eng. Chem. Fundam.* 9 (1970) 283.
- [75] J.R. Ma, *Ind. Eng. Chem. Fundam.* 8 (1969) 560.
- [76] J.R. Ma, *Ind. Eng. Chem. Fundam.* 8 (1969) 564.
- [77] M. Abramowitz and I.A. Stegun, *Handbook of Mathematical Functions* (Nat'l. Bur. Standards, Washington, DC, 1972).
- [78] S.D. Lubetkin and W.J. Dunning, *J. Crystal Growth* 67 (1984) 521.
- [79] R.P. Burns, *J. Chem. Phys.* 44 (1966) 3307.
- [80] C.T. Ewing and K.H. Stern, *J. Phys. Chem.* 79 (1975) 2007.
- [81] H.K. Cammenga, D. Schreiber, G.T. Barnes and D.S. Hunter, *J. Colloid Interface Sci.* 98 (1984) 585.
- [82] K. Tsukamoto, *J. Crystal Growth*, to be published.
- [83] N.-B. Ming, K. Tsukamoto, I. Sunagawa and A.A. Chernov, *J. Crystal Growth* 91 (1988) 11.
- [84] A.A. Chernov, *J. Crystal Growth* 24/25 (1974) 11.
- [85] N. Cho and J. Hallett, *J. Crystal Growth* 69 (1984) 325.
- [86] T. Gonda and T. Koike, *J. Crystal Growth* 65 (1983) 36.